PCCP

PAPER

View Article Online
View Journal | View Issue

Cite this: *Phys. Chem. Chem. Phys.*, 2016, **18**, 14894

Structural effect of glyme–Li^+ salt solvate ionic liquids on the conformation of poly(ethylene oxide)†

Zhengfei Chen,[a] Samila McDonald,[a] Paul A. Fitzgerald,[b] Gregory G. Warr[b] and Rob Atkin*[a]

Received 10th February 2016,
Accepted 10th May 2016

DOI: 10.1039/c6cp00919k

www.rsc.org/pccp

The conformation of 36 kDa polyethylene oxide (PEO) dissolved in three glyme–Li^+ solvate ionic liquids (SILs) has been investigated by small angle neutron scattering (SANS) and rheology as a function of concentration and compared to a previously studied SIL. The solvent quality of a SIL for PEO can be tuned by changing the glyme length and anion type. Thermogravimetric analysis (TGA) reveals that PEO is dissolved in the SILs through Li^+–PEO coordinate bonds. All SILs (lithium triglyme bis(trifluoromethanesulfonyl)imide ([Li(G3)]TFSI), lithium tetraglyme bis(pentafluoroethanesulfonyl)imide ([Li(G4)]BETI), lithium tetraglyme perchlorate ([Li(G4)]ClO_4) and the recently published [Li(G4)]TFSI) are found to be moderately good solvents for PEO but solvent quality decreases in the order [Li(G4)]TFSI ~ [Li(G4)]BETI > [Li(G4)]ClO_4 > [Li(G3)]TFSI due to decreased availability of Li^+ for PEO coordination. For the same glyme length, the solvent qualities of SILs with $TFSI^-$ and $BETI^-$ anions ([Li(G4)]TFSI and [Li(G4)]BETI) are very similar because they weakly coordinate with Li^+, which facilitates Li^+–PEO interactions. [Li(G4)]ClO_4 presents a poorer solvent environment for PEO than [Li(G4)]BETI because ClO_4^- binds more strongly to Li^+ and thereby hinders interactions with PEO. [Li(G3)]TFSI is the poorest PEO solvent of these SILs because G3 binds more strongly to Li^+ than G4. Rheological and radius of gyration (R_g) data as a function of PEO concentration show that the PEO overlap concentrations, c^* and c^{**}, are similar in the three SILs.

Introduction

Ionic liquids (ILs) are salts with melting points below 100 °C. ILs have attracted great research interest owing to their remarkable combination of physicochemical properties including negligible vapour pressure, high ionic conductivity, non-flammability, high thermal stability and large electrochemical window.[1–10]

Solvate ionic liquids (SILs) form when addition of a ligand molecule to a salt results in the formation of complex cations (or anions) and thereby reduces the melting point to less than 100 °C. A series of SILs prepared from mixtures of alkali metal (Li^+, Na^+ and K^+) salts and oligoethers (or glymes, $CH_3(OCH_2CH_2)_nOCH_3$, abbreviated as Gn) have been reported and characterised, in which the glyme molecules coordinate the alkali ions *via* their ether oxygens.[11–18] Li^+ based SILs are attractive electrolytes for secondary lithium ion batteries due to their high lithium content.[19]

In Li^+–glyme SILs, the glyme molecules bind to the Li^+ ion to produce large complex cations. SILs are defined as "good" or "poor" depending on the relative coordination strengths of the glyme and anion with Li^+. In a good SIL, strong and long lived $[Li(glyme)]^+$ cations are formed, resulting in negligible free glyme. Conversely, in a poor SIL, Li^+–anion interactions are stronger than Li^+–glyme interactions, and there can be up to 90% uncoordinated free glyme in the SIL.[14] Good SILs have properties similar to a conventional IL, whereas the properties of poor SILs are like those of concentrated salt solutions.[20] Henderson *et al.* studied the ionic association of different glymes (G1 to G4) in a variety of lithium salts, illustrating the effects of ionic association strength of the salts and the coordinating glyme length on the formation of solvate ionic liquids.[21–23] In general, good SILs are more likely to form when the ionic association strength in the salt is relatively weak. The length of glyme has a more complex effect, however, it appears that the SILs with longer glyme are more stable, as they are more slowly exchangeable.[21]

The structure and interactions of equimolar mixtures of glyme and Li^+ salt (bis(trifluoromethylsulfonyl)imide (TFSI), nitrate or trifluoroacetate salts) have recently been examined using molecular dynamic simulations.[24] It was found that glyme–Li^+ interactions were dominant in the mixture of glyme (G3 or G4)–LiTFSI

[a] *Priority Research Centre for Advanced Fluids and Interfaces, Newcastle Institute for Energy and Resources, The University of Newcastle, Callaghan, NSW 2308, Australia. E-mail: rob.atkin@newcastle.edu.au*
[b] *School of Chemistry, The University of Sydney, Sydney, NSW 2006, Australia*

† Electronic supplementary information (ESI) available. See DOI: 10.1039/c6cp00919k

(good solvate ILs) but were much less in the other two salts. A subsequent experimental study of the bulk structure of a good SIL ([Li(G4)]TFSI) and poor SIL (lithium tetraglyme nitrate ([Li(G4)]NO_3)) has been completed by our group using neutron diffraction and empirical potential structure refinement (EPSR) simulated fits.[18] In [Li(G4)]TFSI, the coordination number between Li^+–G4 is 2–3 times higher than that for Li^+–anion, whereas the coordination number is lower in [Li(G4)]NO_3. This produces Li^+ rich and depleted regions.

Conventional electrolytes in secondary Li^+ batteries are limited by the use of volatile and flammable organic solvents for lithium salts.[25] Polymer electrolytes (PEs) have been explored as replacements for organic solvents due to their negligible volatility and high thermal stability.[26,27] Poly(ethylene oxide) (PEO) is one of the most popular PEs as it is stable to Li^+ metal electrodes. PEO coordinates with Li^+ *via* ether oxygens, which leads to high Li^+ transference numbers.[28–30] However, the conductivities of PEs is only about 10% of typical conventional electrolytes because PEs are usually gels or solids. Recently, researchers have added conventional ILs to PEs in order to improve ionic conductivity and transport properties with some promising results.[29,31] Kido *et al.* recently studied the ionic conductivity of SIL–polymer mixtures, showing greatly enhanced ionic conductivity (by an order of magnitude) compared to conventional PEs.[32] The very high Li^+ content of SILs suggests that their addition to PEs could improve charge storage and overall battery performance in addition to ionic conductivity. Therefore, understanding the mechanism of PEO dissolution in SILs, and how solvent quality varies with changes in the glyme length and anion type, is of both applied and fundamental importance.

The polymer radius of gyration (R_g), which is the average root-mean-squared distance of any point in the polymer coil from its centre of mass, is determined by the solvent quality which is categorised as poor, theta (θ) or good.[33] In a good solvent, polymer chains are expanded (swollen) because interactions between the solvent and the polymer are energetically favourable. In a poor solvent, polymer chains are collapsed as polymer–polymer interactions are preferred over polymer–solvent interactions. In a theta solvent, the excluded volume expansion is cancelled and the chains adopt their random flight conformations (ideal chains). R_g is related to the Flory exponent (ν) by $R_g = K(M_w)^{\nu}$, where K is a constant based on the polymer type and M_w is the polymer molecular weight. Generally, for a good, theta and poor solvent, ν = 0.6, 0.5 and 0.33, respectively.

In moderately good (*i.e.* between a theta and good solvent) or good solvents, polymer solutions can generally be divided into three regimes: dilute, semi-dilute and concentrated regimes.[33] In the dilute regime, the polymer coils are fully swollen by solvent, and R_g is almost independent of concentration. In the semi-dilute regime, there is overlap of neighbouring polymer coils, so R_g decreases with increasing polymer concentration, and the intra-chain excluded volume effect is reduced. In the concentrated regime, R_g is once again relatively constant as a function of polymer concentration. Here the high frequency of inter-chain polymer–polymer interactions means that the theta condition is reached, as the polymer essentially solvates itself. The crossover concentrations from dilute to semi-dilute, and semi-dilute to concentrated, are denoted c^* and c^{**}, respectively.

PEO is soluble in several imidazolium based aprotic ILs[34–40] due to hydrogen bonding with the imidazolium cations.[41] For the protic ILs ethylammonium nitrate (EAN) and propylammonium nitrate (PAN),[42,43] PEO dissolves *via* hydrogen bonding between the ether oxygen and alkylammonium hydrogens. While PAN is a theta solvent for PEO, EAN is a moderately good solvent.

Recently, we reported the first study of PEO conformation dissolved in a SIL, [Li(G4)]TFSI, from the dilute through to the concentrated regime.[44] [Li(G4)]TFSI was found to be a poorer solvent for PEO than water (a good solvent), but better than both EAN and PAN. The solvent quality of the SIL was attributed to coordination bonds between PEO and Li^+, which is very different from both aprotic and protic ILs, where conventional hydrogen bonding is key.[34–38,41,45]

In this work, we examine the relationships between the chemical structure of the SIL and the solvent environment it provides for PEO using small angle neutron scattering (SANS), thermogravimetric analysis (TGA), and rheology. For SANS, at high concentrations, a mixture of hydrogenous and deuterated PEO is used to satisfy zero average contrast (ZAC) conditions, which allows R_g to be extracted despite significant overlap of neighbouring polymer coils.[33,44,46,47] The present study will examine the effect of (1) shortening the glyme length from G4 to G3, (2) increasing the anion size from $TFSI^-$ to bis(pentafluoroethanesulfonyl)imide ($BETI^-$) and (3) employing a poor SIL ([Li(G4)]ClO_4) as the solvent on PEO conformation.

Experimental section

The SILs [Li(G3)]TFSI, [Li(G4)]BETI, and [Li(G4)]ClO_4 were prepared by mixing equimolar triglyme (G3) or tetraglyme (G4) (Sigma Aldrich) with lithium bis(trifluoromethanesulfonyl)imide (Li[TFSI], Sigma Aldrich), lithium bis(pentafluoroethanesulfonyl)imide (Li[BETI], Fluorochem) or lithium perchlorate (Li[ClO_4], Sigma Aldrich), respectively, at 50 °C with constant stirring on a hot plate overnight to form a clear liquid. The SILs were dried at 120 °C for 3 hours. The water contents determined by Karl Fischer titration were 0.02 wt% for [Li(G3)]TFSI, 0.01 wt% for [Li(G4)]BETI and 0.1 wt% for [Li(G4)]ClO_4.

Fully deuterated poly(ethylene oxide) (d-PEO, M_w = 36 kDa, PDI = 1.05) was purchased from Polymer Source (Canada). The corresponding hydrogenous poly(ethylene oxide) (h-PEO, M_w = 34 kDa, PDI = 1.05) was obtained from Fluka. d-PEO–SIL, d,h-PEO–SIL, and h-PEO–SIL solutions from 0.1 to ~11 wt% (1 to 150 mg mL^{-1}) were prepared several days prior to measurement to ensure complete mixing. No phase separation was observed for any sample.

Molecular weights were determined using size exclusion chromatography (SEC) on a Shimadzu CBM-20A liquid chromatography system with an Agilent Polargel-M guard column and three Phenomenex Phenogel 5 μm columns (10e3A/10e4A/10e5A)

at 50 °C. The eluent was dimethylacetamide at a flow rate of 1.0 mL min^{-1}, injections were 100 μL, and detection was with a Shimadzu RID-10A differential refractive index detector. Samples were filtered through a 0.45 μm pore polytetrafluoroethylene (PTFE) membrane prior to injection. The SEC was calibrated with poly(methyl methacrylate) standards (PDI < 1.1), which was adjusted using an 11.4 kDa PEO standard that was predetermined using a Bruker MALDI-TOF mass spectrometer.

Small angle neutron scattering (SANS) experiments were conducted using the QUOKKA beamline[48] at ANSTO (Australia) using 1 mm path-length Hellma Cells. The incident neutron wavelength was 5.0 Å. Two sample-to-detector distances of 2 m and 12 m with count time 30 min and 120 min, respectively, were used to provide a q range of 0.006 to 0.34 $Å^{-1}$. These count times are ~16 times longer than would normally be necessary for deuterated solvents on a high flux instrument such as QUOKKA, but are necessary here because of the high incoherent scattering due to the high hydrogen content of our solvents. After subtraction of the solvent scattering, the uncertainties in scattered intensities are less than 1.5%. Raw 2D SANS data were reduced to 1D data in IGOR Pro with reduction procedures provided by NIST modified for use on QUOKKA.[49] In order to produce the PEO–SIL data on an absolute scale, the empty beam and an empty 1 mm Hellma cell were run before measurement and subtracted from the PEO–SIL SANS data. The pure SILs were run under the same conditions as PEO–SIL solutions and the solvent backgrounds were subtracted from the PEO–SIL solutions during the data reduction process. All experiments were carried out at 25 °C except for the PEO–[Li(G4)]BETI solutions which were analysed at 30 °C to ensure the samples were liquid.

Shear rate dependent viscosities of PEO–SIL solutions were measured on a TA Instruments AR-G2 rheometer using the cone and plate arrangement with a cone of 40 mm diameter and angle of 1°59′36″ by increasing the shear rate from 1 to 1000 s^{-1}. All measurements were maintained at 25 °C except for PEO–[Li(G4)]BETI solutions which were measured at 30 °C. A thermogravimetric analysis (TGA) of 5 wt% PEO in each SIL was performed on a TG/TDA analyser (PerkinElmer) from room temperature to 600 °C at a heating rate of 10 °C min^{-1} under nitrogen gas flow (20 mL min^{-1}).

SANS data analysis

The method for analysing the reduced SANS data was described in detail in the previous work.[44] Generally, the coherent neutron cross section per unit volume, $I(q)$, for solutions of identical deuterated and hydrogenous polymers is given by:[33]

$$I(q)/nN^2 = \varphi(1-\varphi)(b_H - b_D)^2 P(q) + [\varphi b_D + (1-\varphi)b_H - b_s(v_p/v_s)]^2 S(q) \quad (1)$$

where $P(q)$ is the single-chain (intramolecular) form factor, which contains information on R_g, and $S(q)$ is the total scattering structure factor, which describes both intra- and intermolecular correlations between monomer units, and is related to both R_g and the correlation length (ξ). q is the scattering vector expressed as $4\pi\lambda^{-1}\sin\theta$, where λ is the neutron wavelength and 2θ is the scattering angle; n and N are the number density and degree of polymerization of the polymer molecules; b_H, b_D, and b_s are the neutron scattering lengths of the hydrogenous monomer units, deuterated monomer units and the solvent, respectively; v_p/v_s is the ratio of specific volumes for polymer and solvent; and φ is the volume fraction of deuterated polymer chains.

When the polymer chains are fully deuterated (φ = 1), the first term of the right-hand side of eqn (1) is zero. This allows the characteristic dimensions to be determined from $S(q)$. Fits to the data using the polymer excluded volume effect (eqn (2) and (3))[50] yield apparent R_g and the Flory exponent (ν) as a function of polymer concentration. This approach is generally useful in the relatively low polymer concentration regime, but is also used in the concentrated region, see below, where this model reduces to the Debye equation for a Gaussian polymer by setting ν = 0.5 (see eqn (6)).

$$I(q) = \frac{I_0}{\nu U^{\frac{1}{2\nu}}}\gamma\left(\frac{1}{2\nu}, U\right) - \frac{I_0}{\nu U^{\frac{1}{\nu}}}\gamma\left(\frac{1}{\nu}, U\right), \quad (2)$$

where

$$U = \frac{q^2 R_g^2 (2\nu+1)(2\nu+2)}{6} \quad (3)$$

In eqn (2) and (3), I_0 is the scaling factor and $\gamma(x,U)$ is the incomplete gamma function.[50]

The correlation length or "blob size" (ξ), is independent of the molecular weight but decreases with increasing polymer concentration.[51] ξ can be determined from $S(q)$ using the Ornstein–Zernike formula:[52]

$$I(q) = I_0/(1 + q^2\xi^2) \quad (4)$$

Zimm plot analysis allows further insight on the PEO–SIL solutions using the equation:[53]

$$\frac{Kc}{I(q)} \approx \frac{1}{M_w}\left(1 + \frac{q^2 R_g^2}{3}\right) + 2A_2 c \quad (5)$$

where $K = (\Delta\rho/\rho_{PEO})^2 N_A^{-1}$ is the contrast factor, $\Delta\rho$ is the difference in neutron scattering length density between d-PEO and the solvent, ρ_{PEO} is the apparent density of PEO (1.2 g cm^{-3}), N_A is the Avogadro constant, c is the polymer concentration, M_w is the weight-average molecular weight, and A_2 is the second virial coefficient, which indicates the polymer–polymer interactions in a solvent. In general, $A_2 > 0$ for a good solvent due to repulsions between polymers, $A_2 = 0$ for the θ condition and $A_2 < 0$ for a poor solvent due to attractions between polymers.

At higher polymer concentrations, zero average contrast (ZAC) between the polymer and solvent is achieved by mixing hydrogenous and deuterated PEO such that φ = 0.16 for [Li(G3)]TFSI, 0.2 for [Li(G4)]BETI and 0.06 for [Li(G4)]ClO_4 (see ESI,† Table S1 for the neutron scattering length densities). This means that $\varphi b_D + (1-\varphi)b_H = b_s(v_p/v_s)$, so that the second term of the right-hand side of eqn (1) is zero, and R_g is determined from $P(q)$ only. The unperturbed chain dimension in theta condition or melt can be determined by the Debye equation:[33]

$$P(q) = \left(\frac{2}{y^2}\right)[\exp(-y) - 1 + y] + B \quad (6)$$

where $y = q^2{R_g}^2$ and B is the background. It should be noted that R_g determined by the ZAC method is the radius of gyration of an individual chain (real R_g) whereas the R_g from non-ZAC method (bulk contrast) (eqn (2) and (3)) is an "apparent" R_g, but not the R_g of an individual chain.

Results

The SANS patterns for d-PEO dissolved in [Li(G3)]TFSI, [Li(G4)]BETI and [Li(G4)]ClO_4 at PEO concentrations from 1 to 50 mg mL^{-1} are shown in Fig. 1. The SANS spectra for the pure solvents are shown in ESI,† Fig. S1, and are featureless over the q range probed in this work. As expected, the scattering intensity increases with increasing PEO concentration. Data fits using the excluded volume model (eqn (2) and (3)) are also shown in Fig. 1 (solid curves) and the fitting parameters for each system (apparent radius of gyration, R_g, and Flory exponent, ν) are listed in Tables 1–3, respectively, together with correlation lengths, ξ, derived from fits to the Ornstein–Zernike formula (eqn (4)). Fits are shown in the ESI† in Fig. S2.

The apparent R_g of PEO in [Li(G3)]TFSI is 65 Å at 1.5 mg mL^{-1}, and decreases with increasing PEO concentration. The same PEO is slightly more swollen in [Li(G4)]BETI (R_g = 72 Å) and [Li(G4)]ClO_4 (R_g = 71 Å), but these also shrink with increasing concentration (c) across the range examined. Correlation lengths consistently follow the same trend as apparent R_g for all PEO concentrations in these SILs, which is also seen in the aqueous systems.[54] As the polymer concentration increases, more inter-chain interactions occur and adjacent polymer chains are closer together, thus reducing ξ.

At the lowest PEO concentrations examined, the Flory exponents (ν) of 0.513, 0.538, and 0.524 are found for [Li(G3)]TFSI, [Li(G4)]BETI, and [Li(G4)]ClO_4, respectively. At higher PEO concentrations, ν decreases to a near constant value (0.5) with increasing PEO concentration as polymer–polymer interactions increase and solvent–polymer interactions decrease.

These results are also consistent with our previous study of [Li(G4)]TFSI;[44] in the most dilute solutions and at comparable concentrations, apparent R_g of 69 Å, ξ = 45 Å and ν = 0.54 are identical to those found here for [Li(G4)]BETI. This is not surprising given the chemical similarity between the anions.

Zimm plots ($Kc/I(q)$ *vs.* ($q^2 + c$), eqn (5)) for the low concentration SANS data are shown in Fig. 2. Extrapolations to $c = 0$ and $q^2 = 0$ in Fig. 2 are used to determine the fully swollen (infinite dilution) R_g,[55] which are 77 Å, 79 Å and 84 Å for PEO in [Li(G3)]TFSI, [Li(G4)]ClO_4 and [Li(G4)]BETI, respectively, and again close to the previously obtained value of 86 Å in [Li(G4)]TFSI.[44] This confirms that swelling of the PEO chains by the solvent increases in the order [Li(G3)]TFSI < [Li(G4)]ClO_4 < [Li(G4)]BETI ~ [Li(G4)]TFSI, consistent with the Flory exponent values.

Zimm plot analysis also yields second virial coefficients (A_2) between 0.4 and 0.7 × 10^{-3} cm^3 mol g^{-2} for the three SILs. This is consistent with 0.7 × 10^{-3} cm^3 mol g^{-2} obtained in [Li(G4)]TFSI (M_w = 38 kDa PEO),[44] but much smaller than that found in water (A_2 = 2.2 × 10^{-3} cm^3 mol g^{-2}, M_w = 38 kDa PEO)[56] and the aprotic IL [BMIm]BF_4 (A_2 = 2.0 × 10^{-3} cm^3 mol g^{-2}, M_w = 27.3 kDa PEO),[39]

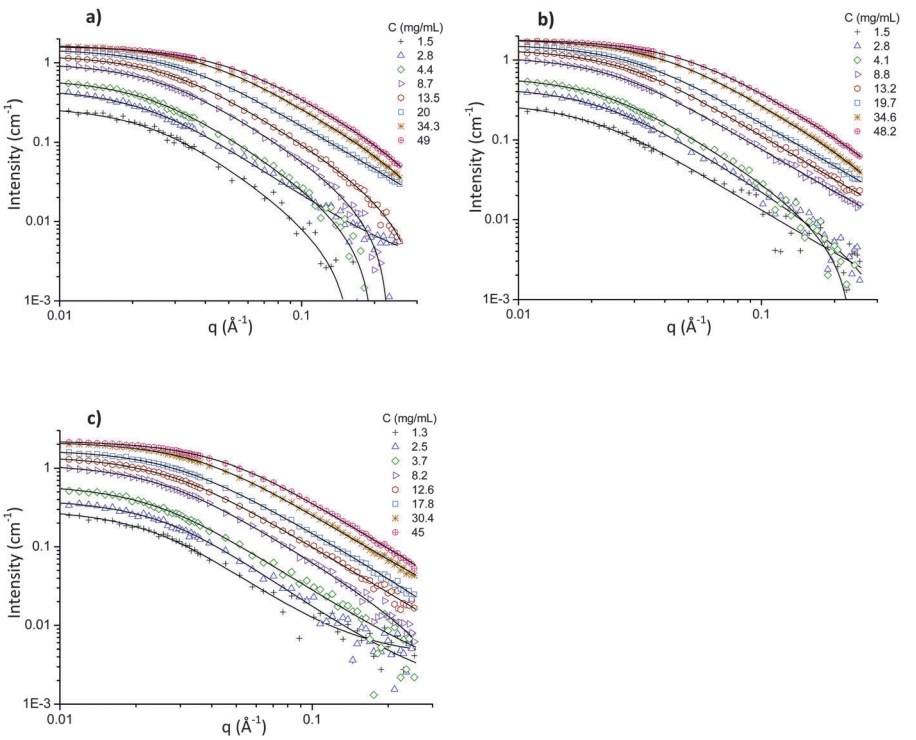

Fig. 1 SANS intensity for (a) d-PEO–[Li(G3)]TFSI, (b) d-PEO–[Li(G4)]BETI and (c) d-PEO–[Li(G4)]ClO_4 solutions of varying PEO concentration with background subtracted. Lines are polymer excluded volume model fits to the data.

Table 1 Fitted apparent radius of gyration, R_g, correlation length, ξ and Flory exponent, ν for d-PEO–[Li(G3)]TFSI solutions

d-PEO conc. (mg mL^{-1})	Apparent R_g (Å)	ξ (Å)	ν
1.5	65	43	0.513
2.8	66	43	0.515
4.4	62	41	0.505
8.7	55	37	0.505
13.5	50	33	0.505
20.0	44	29	0.505
34.3	35	23	0.505
49.0	29	19	0.505

Table 2 Fitted apparent radius of gyration, R_g, correlation length, ξ and Flory exponent, ν for d-PEO–[Li(G4)]BETI solutions

d-PEO conc. (mg mL^{-1})	Apparent R_g (Å)	ξ (Å)	ν
1.5	72	48	0.538
2.8	66	43	0.529
4.1	64	42	0.515
8.8	58	38	0.526
13.2	52	34	0.521
19.7	47	30	0.524
34.6	37	24	0.513
48.2	30	19	0.513

Table 3 Fitted apparent radius of gyration, R_g, correlation length, ξ and Flory exponent, ν for d-PEO–[Li(G4)]ClO_4 solutions

d-PEO conc. (mg mL^{-1})	Apparent R_g (Å)	ξ (Å)	ν
1.3	71	48	0.524
2.5	65	42	0.524
3.7	66	43	0.524
8.2	58	39	0.510
12.6	54	36	0.510
17.8	48	32	0.515
30.4	41	27	0.513
45.0	34	23	0.503

which are good solvents for PEO. However, the solvent quality of these SILs is better than that of the protic IL EAN, which has a much smaller A_2 value of 1.6×10^{-6} cm^3 mol g^{-2} (M_w = 38 kDa PEO), and is closer to a theta solvent for PEO.[43] Therefore, our analysis reveals that SILs are moderately good solvents for PEO.

At high PEO concentrations, R_g cannot be determined through the excluded volume model because of inter-chain interactions,[47] so the zero average contrast (ZAC) method is used. SANS results for PEO in [Li(G3)]TFSI, [Li(G4)]BETI and [Li(G4)]ClO_4 at PEO concentrations from 50 to 150 mg mL^{-1} with corresponding fits to the Debye model (eqn (6)) are shown in Fig. 3, with best-fit parameters listed in Table 4.

At high PEO concentrations, $R_g = 65 \pm 2$ Å is independent of the SIL and PEO concentration within experimental uncertainty. The R_g value ($\sim 65 \pm 2$ Å) for the PEO is close to the measured chain size of 70 Å for the same M_w in the melt,[57] indicating that these solutions in the concentrated regime have already achieved the limiting R_g value for that of the melt. Viscosities of PEO–SIL solutions at various PEO concentrations were measured as a function of shear rate from 1 to 1000 s^{-1} (see ESI,† Fig. S3). The viscosities of pure [Li(G3)]TFSI, [Li(G4)]BETI and [Li(G4)]ClO_4 are consistent with previous reports.[15] For the SIL–PEO systems, viscosity increases notably with increasing PEO concentration, and slight shear thinning was observed at shear rates above 200 s^{-1}. This is typical for PEO in various ILs such as EAN and PAN,[58] and also in water,[59] but the microscopic explanation of shear thinning is still a matter of debate.[60]

The c^* and c^{**} concentrations, which define the transitions from the dilute to semi-dilute and semi-dilute to concentrated regimes, can be determined from slope changes in plots of apparent R_g, ξ, or viscosity as a function of polymer concentration.[44] In Fig. 4, apparent R_g and ξ for PEO decrease slightly at low PEO concentrations, then follows an apparent $R_g \sim c^{-0.25}$ dependence at higher PEO concentrations. Note that this is an apparent R_g, and is not expected to follow $R_g \sim c^{-0.125}$,[61] as stated in the experimental section. The concentration at which the slope changes is c^*, and gives values of 16, 12 and 14 mg mL^{-1} for [Li(G3)]TFSI, [Li(G4)]BETI and [Li(G4)]ClO_4 respectively. These experimental values can be compared to c^* values calculated from R_g at infinite dilution using $c^* = (M_w/N_A)/(4\pi {R_g}^3/3)$, and give corresponding values of 31, 24 and 29 mg mL^{-1} respectively. The experimental values are about a factor of two smaller than the calculated values, but within the difference of about one experimental data point. R_g at higher PEO concentrations is determined from ZAC data, which enabled c^{**} to be measured at 50, 43 and 45 mg mL^{-1} for [Li(G3)]TFSI, [Li(G4)]BETI and [Li(G4)]ClO_4 respectively.

Viscosity as a function of polymer concentration is also shown in Fig. 4 for the three PEO–SIL systems. In the dilute regime, viscosity increases weakly with polymer concentration as chains are mostly isolated. In the semi-dilute regime, the viscosity increases more steeply due to increasing entanglement of polymer chains. In the concentrated regime, the polymer–polymer interactions are dominant, which results in a much sharper increase in the viscosity with increasing concentration. The crossovers c^* (from dilute to semi-dilute) and c^{**} (from semi-dilute to concentrated), determined from the viscosity trend agree very well with those determined from R_g, as shown in Fig. 4.

For the same polymer, better solvent quality leads to a smaller c^* and c^{**} as the polymer chains are more extended. The crossover concentrations therefore show that the solvent quality for PEO increases in the order of [Li(G3)]TFSI < [Li(G4)]ClO_4 < [Li(G4)]TFSI $\sim$ [Li(G4)]BETI. The c^* for the same PEO polymer in EAN was reported as between 24 and 60 mg mL^{-1},[43] suggesting that EAN is a poorer solvent than the SILs.

TGA curves for 5 wt% PEO in pure glyme (G3 or G4) and the three SILs are shown in Fig. 5. The data for PEO in G3 and G4 are similar to that for the pure glymes[15] until the decomposition temperatures of 167 °C for G3 and 206 °C for G4 are reached.[15] Above these temperatures, approximately 5 wt% of the total mass (PEO polymer) is retained until the PEO begins to decompose at $\sim$340 °C. This confirms no strong interactions between PEO and the pure glymes, consistent with only weak dispersion interactions between ethylene oxide groups.

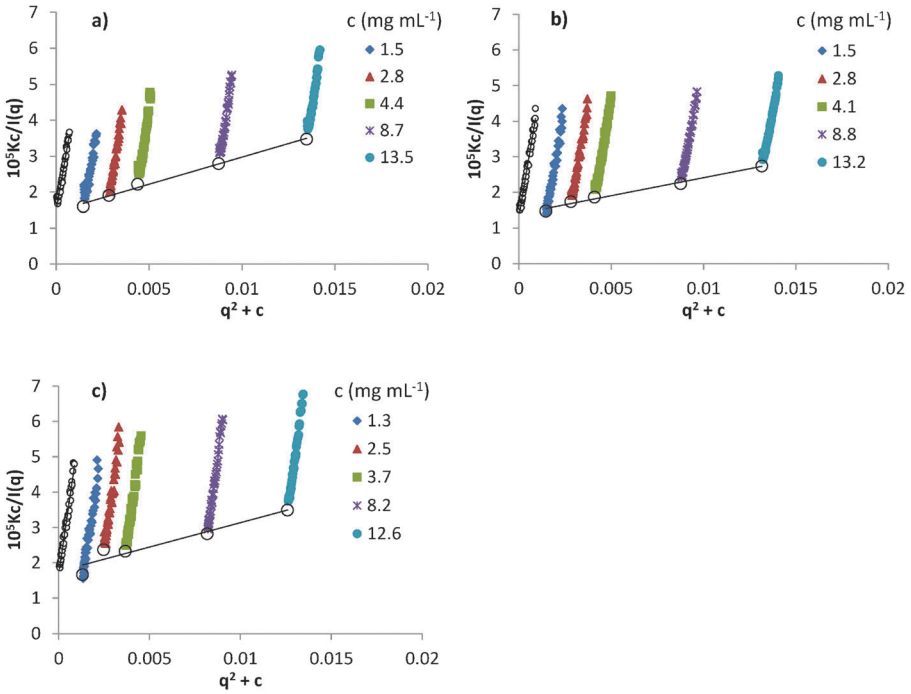

Fig. 2 Zimm plots of d-PEO–SIL solutions at PEO concentrations between 1 and 15 mg mL^{-1} in: (a) [Li(G3)]TFSI, (b) [Li(G4)]BETI and (c) [Li(G4)]ClO_4. Small open circles and large open circles are the extrapolation of the SANS data to c = 0 and q^2 = 0, respectively.

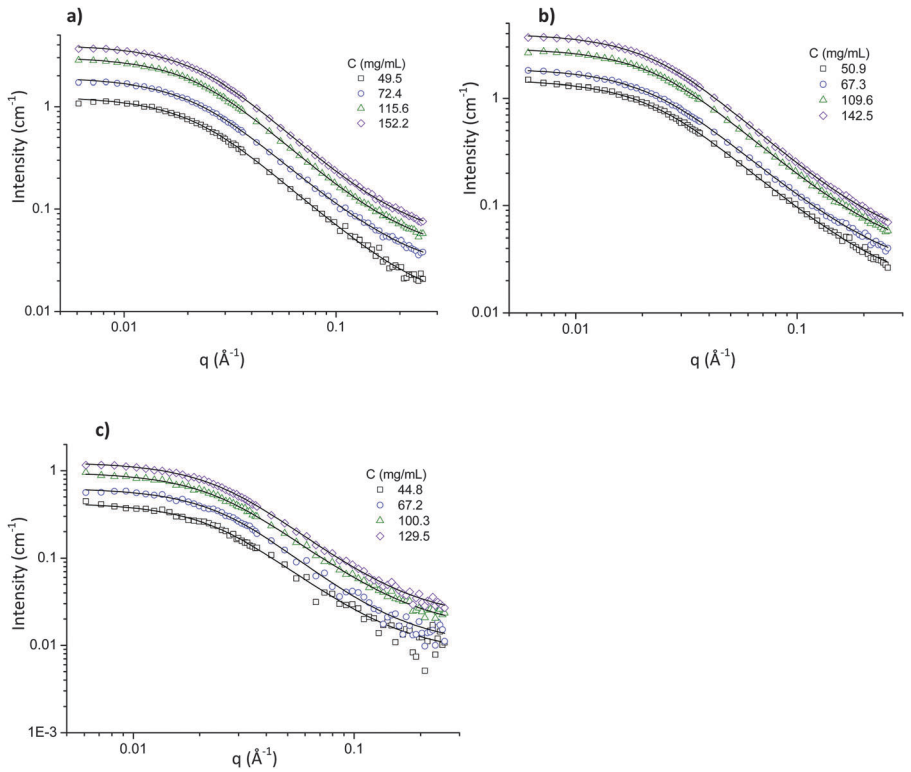

Fig. 3 SANS intensity at ZAC for (a) PEO–[Li(G3)]TFSI, (b) PEO–[Li(G4)]BETI and (c) PEO–[Li(G4)]ClO_4 solutions of varying PEO concentration with background subtracted. Lines are Debye model fits to the data.

TGA profiles for the PEO–SILs solutions are similar to those of pure SILs[15] over the entire temperature range. All PEO–SIL solutions exhibit thermal stability up to ~200 °C, as shown in Fig. 5. For PEO in the good SILs, [Li(G3)]TFSI and [Li(G4)]BETI, there is a gradual decrease in weight due to glyme decomposition above 200 °C and PEO above 350 °C until almost all mass is

Table 4 Fitted radius of gyration, R_g, for PEO–SIL solutions under ZAC conditions

PEO–[Li(G3)]TFSI		PEO–[Li(G4)]BETI		PEO–[Li(G4)]ClO_4	
PEO conc. (mg mL^{-1})	R_g (Å)	PEO conc. (mg mL^{-1})	R_g (Å)	PEO conc. (mg mL^{-1})	R_g (Å)
49.5	66	50.9	63	44.8	66
72.4	65	67.2	62	70	64
115.6	65	100.3	60	110	64
152.2	64	129.5	62	140	64

lost at ~420 °C. The remaining mass is residual carbon. For the PEO in the poor SIL [Li(G4)]ClO_4, weight loss is more rapid above 200 °C due to the markedly greater amount of free glyme.[15] At 341 °C, 30 wt% of the original mass remains, which is equal to the sum of PEO and $LiClO_4$, *i.e.* all of the glyme has been removed. At higher temperatures, PEO begins to decompose, and $LiClO_4$ decomposition commences at 390 °C.[62] The 12 wt% mass fraction present at temperatures greater than 470 °C and its white appearance is consistent with decomposition of $LiClO_4$ into LiCl.[62]

Discussion

The conformation of a polymer in solution is dictated by the solvent quality, which is governed by the balance of polymer–polymer and polymer–solvent interactions. Fits to the SANS data (R_g coil size and R_g at infinite dilution, Flory exponent ν) revealed that the three SILs are moderately good solvents, with solvent quality increasing in the order [Li(G3)]TFSI < [Li(G4)]ClO_4 < [Li(G4)]TFSI ~ [Li(G4)]BETI. Trends in viscosity as a function of concentration confirm this order.

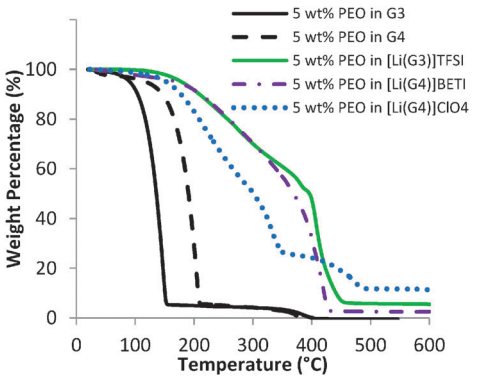

Fig. 5 TGA curves of 5 wt% PEO in pure glymes and SILs under N_2 flow. Note: the 5 wt% PEO in G4 data (dashed line) was reproduced from our previous work[44] for comparison.

[Li(G3)]TFSI is a poorer solvent for PEO than either [Li(G4)]TFSI or [Li(G4)]BETI. In pure Li^+–glyme SILs, the glyme molecules compete with the anion for Li^+.[14,15] It has previously been shown that the Li^+–O distance of ~2.2 Å in [Li(G4)]TFSI is reduced to ~2.0 Å in [Li(G3)]TFSI,[16] indicating tighter Li^+–glyme binding. Tighter binding leads to higher ionicity (cation–anion separation)[16,63] and higher viscosity.[15,63] For PEO to be solvated by the SIL it must compete effectively for Li^+ coordination sites with both the glyme and anion. Molecular Dynamics simulations have shown that the number of anions not attached to any Li^+ doubles from 6% in [Li(G3)]TFSI to 12.2% in [Li(G4)]TFSI,[24] meaning that anions are more strongly associated with Li^+ in [Li(G3)]TFSI. Tighter binding of G3 to Li^+ than G4 means that Li^+ is less available to bind PEO, resulting in poorer solvency.

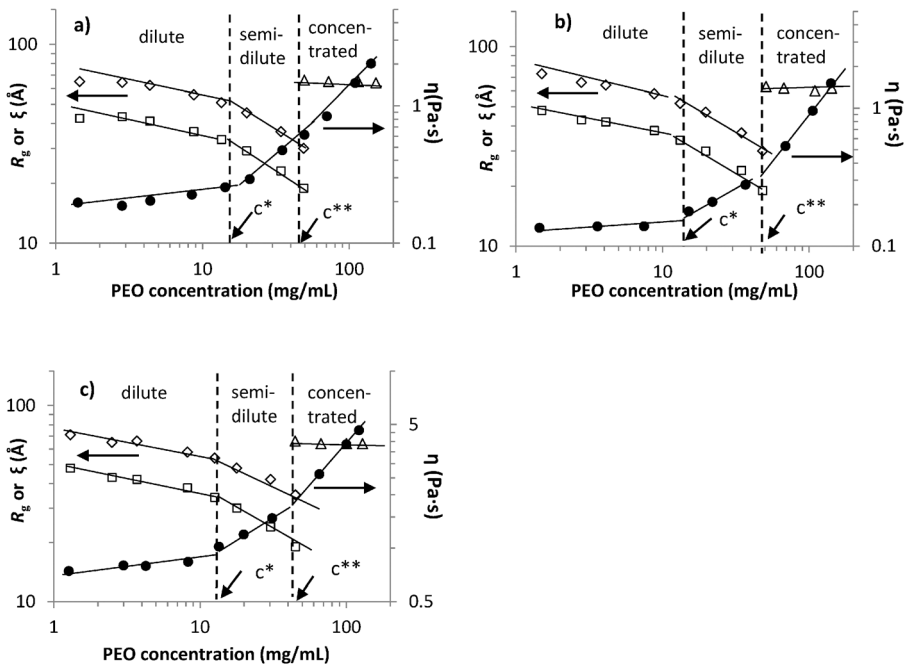

Fig. 4 Apparent radius of gyration, R_g, and correlation length, ξ as function of PEO concentration determined by SANS and viscosity of PEO–SIL solutions at various PEO concentrations in (a) [Li(G3)]TFSI, (b) [Li(G4)]BETI and (c) [Li(G4)]ClO_4. ◇: R_g at bulk contrast; □: ξ; △: R_g at ZAC; ●: rheology, η.

Employing the same glyme length enables the effect of the anion on PEO solvation to be assessed. The solvent quality for PEO for G4 based SILs is [Li(G4)]TFSI ~ [Li(G4)]BETI > [Li(G4)]ClO_4. Henderson *et al.* reported the association strength for LiX salts in glymes is $BETI^-$ ~ $TFSI^-$ < ClO_4^-.[21] This means ClO_4^- coordinates much more strongly to Li^+ than the other two anions. While $BETI^-$ is slightly larger than $TFSI^-$ due to its two additional CF_2 groups, it has similar coordination strength. Therefore, Li^+ is similarly available to bind with PEO in [Li(G4)]TFSI and [Li(G4)]BETI, but less so in [Li(G4)]ClO_4, consistent with the trends in solvent quality.

The solvent quality of PEO dissolved in its monomeric liquids, ethylene glycol and monoglyme has been studied using rheology and photon correlation spectroscopy (PCS).[64] The polymer–solvent and solvent–solvent interactions were greatly influenced by the number of H-bond donors available in the solvent, with increased H-bond capacity leading to better solvency. This is consistent with our observations. Given that lithium acts a hydrogen bond donor, as the Li^+ concentration per unit volume increases (from [Li(G4)]ClO_4 to [Li(G4)]TFSI and [Li(G4)]BETI) the solvent quality increases.

Strong coordination of ClO_4^- with Li^+ means that [Li(G4)]ClO_4 is a poor SIL, with around 20% free glyme.[14] This means PEO in [Li(G4)]ClO_4 can be solvated by both free glyme as well as complex cation and anion. Given that the TGA data confirms that interaction between G4 and PEO are weak, this will also contribute to [Li(G4)]ClO_4 being a poorer solvent.

Coordination between the Li and glyme leads to a greater thermal stability for the three SILs up to ~200 °C.[14,15] For PEO–[Li(G4)]ClO_4, the more severe mass loss is due to the weaker coordination between glyme and Li^+.[15] At 341 °C, 30 wt% of the mass is retained which is equal to the sum of PEO and $LiClO_4$. The great similarity in the thermal behaviour between the PEO–SIL solutions and their respective SILs suggests that PEO does not completely replace the glyme from Li^+,[44] irrespective of the change of the structure on the SIL.

We argued in our previous work that the dissolution of PEO in [Li(G4)]TFSI was *via* the coordination between Li^+ and PEO.[44] Typical coordination numbers for LiX–PEO complexes are 4 to 6.[65,66] Recent molecular dynamics simulations suggest that the average coordination number (Li^+/O) in both [Li(G3)]TFSI and [Li(G4)]TFSI is 5, with 1 and 0.5 oxygens contributed from the anion, respectively.[13] Therefore, in SILs such as [Li(G3)]TFSI and [Li(G4)]TFSI, it is more likely that PEO is solvated by displacing the anion from the coordination sphere of lithium ions, and we expect that solvation in [Li(G4)]BETI will be similar. The recent work on thermal, ionic and electrochemical properties of PEO–[Li(G4)]TFSI by Kido *et al.* showed that some Li–PEO complex could also form,[32] which may effect the PEO structure.

Conclusions

PEO is dissolved in [Li(G3)]TFSI, [Li(G4)]BETI and [Li(G4)]ClO_4 *via* the coordination between PEO ether oxygens and Li^+, although interactions between PEO and free glyme may also play a role in [Li(G4)]ClO_4. All three solvate ionic liquids are moderately good solvents for PEO as revealed by the Flory exponent values, Zimm analysis, and viscosity behaviour.

Solvent quality increases in the order of [Li(G3)]TFSI < [Li(G4)]ClO_4 < [Li(G4)]BETI ~ [Li(G4)]TFSI. The R_g values and the crossover concentrations determined from trends in R_g and viscosity as a function of PEO concentration show that PEO conformation in the SILs is similar, and much less affected by changing ion structures compared to that in common ionic liquids.[67] This is likely a consequence of the mechanism of solvation being coordination bonds with Li^+ ions in SILs rather than hydrogen bonds in conventional ILs.

PEO must compete with anion and glyme for Li^+ coordination sites to be solvated. If there is a stronger coordination between Li^+ and the anion (ClO_4^- *vs.* $TFSI^-$ or $BETI^-$) or Li^+ and glyme (*e.g.* G3 *vs.* G4), then the solvent quality is poorer for PEO. For the same glyme length, weakly coordinating anions (good SILs) are better solvents than strongly coordinating anions (poor SILs) because the lithium ion is more available for binding PEO. The poor SIL contains a substantial proportion of free glyme which could also contribute to poorer solvation because glyme–PEO interactions are weak.

Acknowledgements

GGW and RA acknowledge support from Australian Research Council Discovery Projects, and RA acknowledges ARC for a Future Fellowship. The authors wish to thank ANSTO for the provision of small angle neutron scattering beamtime (Proposal 4452). This work benefitted from software developed by the DANSE project under NSF award DMR-0520547.

References

1 T. Welton, *Coord. Chem. Rev.*, 2004, **248**, 2459–2477.
2 D. R. MacFarlane, N. Tachikawa, M. Forsyth, J. M. Pringle, P. C. Howlett, G. D. Elliott, J. H. Davis, M. Watanabe, P. Simon and C. A. Angell, *Energy Environ. Sci.*, 2014, **7**, 232–250.
3 Z. Chen, P. A. FitzGerald, Y. Kobayashi, K. Ueno, M. Watanabe, G. G. Warr and R. Atkin, *Macromolecules*, 2015, **48**, 1843–1851.
4 Z. Chen, Y. Kobayashi, G. B. Webber, K. Ueno, M. Watanabe, G. G. Warr and R. Atkin, *Langmuir*, 2015, **31**, 7025–7031.
5 T. L. Greaves and C. J. Drummond, *Chem. Soc. Rev.*, 2008, **37**, 1709–1726.
6 A. Dolan, R. Atkin and G. G. Warr, *Chem. Sci.*, 2015, **6**, 6189–6198.
7 R. Hayes, G. G. Warr and R. Atkin, *Chem. Rev.*, 2015, **115**, 6357–6426.
8 J. Sweeney, G. B. Webber and R. Atkin, *Phys. Chem. Chem. Phys.*, 2015, **17**, 26629–26637.

9 D. Wakeham, P. Niga, C. Ridings, G. Andersson, A. Nelson, G. G. Warr, S. Baldelli, M. W. Rutland and R. Atkin, *Phys. Chem. Chem. Phys.*, 2012, **14**, 5106–5114.
10 O. Werzer and R. Atkin, *Phys. Chem. Chem. Phys.*, 2011, **13**, 13479–13485.
11 T. Mandai, K. Yoshida, S. Tsuzuki, R. Nozawa, H. Masu, K. Ueno, K. Dokko and M. Watanabe, *J. Phys. Chem. B*, 2015, **119**, 1523–1534.
12 T. Tamura, T. Hachida, K. Yoshida, N. Tachikawa, K. Dokko and M. Watanabe, *J. Power Sources*, 2010, **195**, 6095–6100.
13 S. Tsuzuki, W. Shinoda, M. Matsugami, Y. Umebayashi, K. Ueno, T. Mandai, S. Seki, K. Dokko and M. Watanabe, *Phys. Chem. Chem. Phys.*, 2015, **17**, 126–129.
14 K. Ueno, R. Tatara, S. Tsuzuki, S. Saito, H. Doi, K. Yoshida, T. Mandai, M. Matsugami, Y. Umebayashi, K. Dokko and M. Watanabe, *Phys. Chem. Chem. Phys.*, 2015, **17**, 8248–8257.
15 K. Ueno, K. Yoshida, M. Tsuchiya, N. Tachikawa, K. Dokko and M. Watanabe, *J. Phys. Chem. B*, 2012, **116**, 11323–11331.
16 K. Yoshida, M. Nakamura, Y. Kazue, N. Tachikawa, S. Tsuzuki, S. Seki, K. Dokko and M. Watanabe, *J. Am. Chem. Soc.*, 2011, **133**, 13121–13129.
17 B. McLean, H. Li, R. Stefanovic, R. J. Wood, G. B. Webber, K. Ueno, M. Watanabe, G. G. Warr, A. Page and R. Atkin, *Phys. Chem. Chem. Phys.*, 2015, **17**, 325–333.
18 T. Murphy, S. K. Callear, N. Yepuri, K. Shimizu, M. Watanabe, J. N. Canongia Lopes, T. Darwish, G. G. Warr and R. Atkin, *Phys. Chem. Chem. Phys.*, 2016, DOI: 10.1039/C6CP00176A.
19 C. Zhang, A. Yamazaki, J. Murai, J.-W. Park, T. Mandai, K. Ueno, K. Dokko and M. Watanabe, *J. Phys. Chem. C*, 2014, **118**, 17362–17373.
20 T. Mandai, K. Yoshida, K. Ueno, K. Dokko and M. Watanabe, *Phys. Chem. Chem. Phys.*, 2014, **16**, 8761–8772.
21 W. A. Henderson, *J. Phys. Chem. B*, 2006, **110**, 13177–13183.
22 W. A. Henderson, N. R. Brooks, W. W. Brennessel and V. G. Young, *Chem. Mater.*, 2003, **15**, 4679–4684.
23 W. A. Henderson, N. R. Brooks and V. G. Young, *Chem. Mater.*, 2003, **15**, 4685–4690.
24 K. Shimizu, A. A. Freitas, R. Atkin, G. G. Warr, P. A. FitzGerald, H. Doi, S. Saito, K. Ueno, Y. Umebayashi, M. Watanabe and J. N. Canongia Lopes, *Phys. Chem. Chem. Phys.*, 2015, **17**, 22321–22335.
25 K. Xu, *Chem. Rev.*, 2014, **114**, 11503–11618.
26 D. T. Hallinan and N. P. Balsara, *Annu. Rev. Mater. Res.*, 2013, **43**, 503–525.
27 W. H. Meyer, *Adv. Mater.*, 1998, **10**, 439–448.
28 E. Quartarone, P. Mustarelli and A. Magistris, *Solid State Ionics*, 1998, **110**, 1–14.
29 J. H. Shin, W. A. Henderson and S. Passerini, *J. Electrochem. Soc.*, 2005, **152**, A978–A983.
30 J. Xi, X. Qiu, M. Cui, X. Tang, W. Zhu and L. Chen, *J. Power Sources*, 2006, **156**, 581–588.
31 J.-H. Shin, W. A. Henderson and S. Passerini, *Electrochem. Commun.*, 2003, **5**, 1016–1020.
32 R. Kido, K. Ueno, K. Iwata, Y. Kitazawa, S. Imaizumi, T. Mandai, K. Dokko and M. Watanabe, *Electrochim. Acta*, 2015, **175**, 5–12.
33 G. Cheng, W. W. Graessley and Y. B. Melnichenko, *Phys. Rev. Lett.*, 2009, **102**, 157801.
34 H.-N. Lee and T. P. Lodge, *J. Phys. Chem. Lett.*, 2010, **1**, 1962–1966.
35 S. K. Chaurasia, R. K. Singh and S. Chandra, *J. Raman Spectrosc.*, 2011, **42**, 2168–2172.
36 L. T. Costa and M. C. C. Ribeiro, *J. Chem. Phys.*, 2006, **124**, 184902.
37 J. M. Harner and D. A. Hoagland, *J. Phys. Chem. B*, 2010, **114**, 3411–3418.
38 Z. F. Bai, M. W. Nagy, B. Zhao and T. P. Lodge, *Langmuir*, 2014, **30**, 8201–8208.
39 A. Triolo, O. Russina, U. Keiderling and J. Kohlbrecher, *J. Phys. Chem. B*, 2006, **110**, 1513–1515.
40 H.-N. Lee, N. Newell, Z. Bai and T. P. Lodge, *Macromolecules*, 2012, **45**, 3627–3633.
41 N. Winterton, *J. Mater. Chem.*, 2006, **16**, 4281–4293.
42 J. A. Smith, G. B. Webber, G. G. Warr, A. Zimmer, R. Atkin and O. Werzer, *J. Colloid Interface Sci.*, 2014, **430**, 56–60.
43 O. Werzer, G. G. Warr and R. Atkin, *J. Phys. Chem. B*, 2011, **115**, 648–652.
44 Z. Chen, P. A. FitzGerald, G. G. Warr and R. Atkin, *Phys. Chem. Chem. Phys.*, 2015, **17**, 14872–14878.
45 J. Mondal, E. Choi and A. Yethiraj, *Macromolecules*, 2014, **47**, 438–446.
46 J. S. King, W. Boyer, G. D. Wignall and R. Ullman, *Macromolecules*, 1985, **18**, 709–718.
47 M. Benmouna and B. Hammouda, *Prog. Polym. Sci.*, 1997, **22**, 49–92.
48 E. P. Gilbert, J. C. Schulz and T. J. Noakes, *Phys. B*, 2006, **385–386**(part 2), 1180–1182.
49 S. R. Kline, *J. Appl. Crystallogr.*, 2006, **39**, 895–900.
50 B. Hammouda, *Adv. Polym. Sci.*, 1993, **106**, 87–133.
51 M. Adam and M. Delsanti, *Macromolecules*, 1977, **10**, 1229–1237.
52 H. E. Stanley, *Introduction to Phase Transitions and Critical Phenomena*, Oxford University Press, Oxford, 1971.
53 B. H. Zimm, *J. Chem. Phys.*, 1945, **13**, 141–145.
54 B. Hammouda and D. L. Ho, *J. Polym. Sci., Part B: Polym. Phys.*, 2007, **45**, 2196–2200.
55 C. B. Shogbon, J.-L. Brousseau, H. Zhang, B. C. Benicewicz and Y. A. Akpalu, *Macromolecules*, 2006, **39**, 9409–9418.
56 K. Devanand and J. C. Selser, *Macromolecules*, 1991, **24**, 5943–5947.
57 L. J. Fetters, D. J. Lohse, D. Richter, T. A. Witten and A. Zirkel, *Macromolecules*, 1994, **27**, 4639–4647.
58 J. A. Smith, G. B. Webber, G. G. Warr and R. Atkin, *J. Phys. Chem. B*, 2013, **117**, 13930–13935.
59 V. Gauri and K. Koelling, *Rheol. Acta*, 1997, **36**, 555–567.
60 X. Xu, J. Chen and L. An, *J. Chem. Phys.*, 2014, **140**, 174902.
61 M. Daoud, J. P. Cotton, B. Farnoux, G. Jannink, G. Sarma, H. Benoit, C. Duplessix, C. Picot and P. G. de Gennes, *Macromolecules*, 1975, **8**, 804–818.

62 K. H. Stern, *J. Phys. Chem. Ref. Data*, 1974, **3**, 481–526.
63 T. Tamura, K. Yoshida, T. Hachida, M. Tsuchiya, M. Nakamura, Y. Kazue, N. Tachikawa, K. Dokko and M. Watanabe, *Chem. Lett.*, 2010, **39**, 753–755.
64 V. Crupi, A. Faraone, G. Maisano, D. Majolino, P. Migliardo, V. Venuti and V. Villari, *J. Chem. Phys.*, 2000, **112**, 5205–5211.
65 J. D. Londono, B. K. Annis, A. Habenschuss, O. Borodin, G. D. Smith, J. Z. Turner and A. K. Soper, *Macromolecules*, 1997, **30**, 7151–7157.
66 G. Mao, M.-L. Saboungi, D. L. Price, M. B. Armand and W. S. Howells, *Phys. Rev. Lett.*, 2000, **84**, 5536–5539.
67 T. Ueki and M. Watanabe, *Bull. Chem. Soc. Jpn.*, 2012, **85**, 33–50.